A Carboxylate Oxygen of the Substrate Bridges the Magnesium Ions at the Active Site of Enolase: Structure of the Yeast Enzyme Complexed with the Equilibrium Mixture of 2-Phosphoglycerate and Phosphoenolpyruvate at 1.8 Å Resolution[†,‡]

Todd M. Larsen, Joseph E. Wedekind,[§] Ivan Rayment,* and George H. Reed*

Institute for Enzyme Research, Graduate School, and Department of Biochemistry, College of Agricultural and Life Sciences, University of Wisconsin—Madison, Madison, Wisconsin 53705

Received December 4, 1995; Revised Manuscript Received February 1, 1996[⊗]

ABSTRACT: The equilibrium mixture of yeast enolase with substrate, 2-phospho-D-glycerate (2-PGA), and product, phosphoenolpyruvate (P-enolpyruvate), has been crystallized from solutions of poly(ethylene glycol) (PEG) at pH 8.0. Crystals belong to the space group *C*2 and have unit cell dimensions $a = 121.9$ Å, $b = 73.2$ Å, $c = 93.9$ Å, and $\beta = 93.3°$. The crystals have one dimer per asymmetric unit. Crystals of the equilibrium mixture and of the enolase complex of phosphonoacetohydroxamate (PhAH) are isomorphous, and the structure of the former complex was solved from the coordinates of enolase−$(Mg^{2+})_2$−PhAH [Wedekind, J. E., Poyner, R. R., Reed, G. H., & Rayment, I. (1994) *Biochemistry 33*, 9333−9342]. The current crystallographic *R*-factor is 17.7% for all recorded data (92% complete) to 1.8 Å resolution. The electron density map is unambiguous with respect to the positions and liganding of both magnesium ions and with respect to the stereochemistry of substrate/product binding. Both magnesium ions are complexed to functional groups of the substrate/product. The higher affinity Mg^{2+} coordinates to the carboxylate side chains of Asp 246, Glu 295, and Asp 320, both carboxylate oxygens of the substrate/product, and a water molecule. One of the carboxylate oxygens of the substrate/product also coordinates to the lower affinity Mg^{2+}—thus forming a μ-carboxylato bridge. The other ligands of the second Mg^{2+} are a phosphoryl oxygen of the substrate/product, two water molecules, and the carbonyl and γ -oxygens of Ser 39 from the active site loop. The intricate coordination of both magnesium ions to the carboxylate group suggests that both metal ions participate in stabilizing negative charge in the carbanion (*aci*-carboxylate) intermediate. The ϵ-amino group of Lys 345 is positioned to serve as the base in the forward reaction whereas the carboxylate side chain of Glu 211 is positioned to interact with the 3-OH of 2-PGA. The structure provides a candid view of the catalytic machinery of enolase.

Enolase catalyzes the reversible elimination of water from 2-PGA[1] to give P-enolpyruvate. The reaction proceeds with *anti* stereochemistry (Cohn et al., 1970) and has an equilibrium constant of ∼4 off and ∼1 on the enzyme (Burbaum & Knowles, 1989). Early isotope exchange experiments of Dinovo and Boyer (1971) suggested that the reaction is stepwise (Scheme 1). In the forward direction, an enzymic base removes a proton from C-2 of 2-PGA creating a carbanion (or *aci*-carboxylate) intermediate. For enolase, this ionization step constitutes a substantial barrier because the C-2 proton has a pK_a estimated to be >30, and such carbon acids are known to undergo slow ionization. The second

Scheme 1

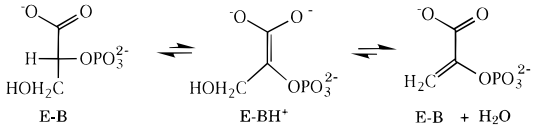

and last bond breaking step is loss of OH^- from the hydroxymethyl group of the intermediate to give P-enolpyruvate. This stepwise reaction mechanism is supported by several subsequent experiments (Stubbe & Abeles, 1980; Anderson et al., 1984, 1994; Poyner et al., 1996). Generation of carbanion (enolate) intermediates adjacent to carboxylate or carbonyl functions is believed to be the initial step in numerous enzyme-catalyzed elimination and isomerization reactions. The mechanisms for generation of these intermediates are of current interest (Gerlt & Gassman, 1992, 1993; Guthrie & Kluger, 1993). This interest is heightened by recognition of a high degree of sequence and structural similarity within a family of enzymes catalyzing such reactions (Petsko et al., 1993; Wedekind et al., 1995; Babbitt et al., 1995).

The divalent metal ion requirement of enolase was recognized early on (Wold & Ballou, 1957; Malmström, 1961), although the metal ion stoichiometry—2 equiv of divalent cation per subunit for full activity—was firmly established much later (Faller et al., 1977). The metal ion

[†] This research was supported in part by NIH Grants GM35752 (G.H.R.) and AR35186 (I.R.) and by an NRSA Fellowship (J.E.W.) from NIH Training Grant GM08293.

[‡] X-ray coordinates for this complex of enolase have been deposited in the Brookhaven Protein Data Bank under file name 1ONE.

* Corresponding authors.

[§] Present address: Department of Structural Biology, Fairchild Center, Stanford University School of Medicine, Stanford, CA 94305-5400.

[⊗] Abstract published in *Advance ACS Abstracts,* March 15, 1996.

[1] Abbreviations: 2-PGA, 2-phospho-D-glycerate; P-enolpyruvate, phosphoenolpyruvate; HEPPS, *N*-(2-hydroxyethyl)piperazine-*N*′-3-propanesulfonic acid; TSP, tartronate semialdehyde phosphate; PhAH, phosphonoacetohydroxamate; PEG, poly(ethylene glycol); NMR, nuclear magnetic resonance; EPR, electron paramagnetic resonance; (*Z*)-3-Cl-P-enolpyruvate, (*Z*)-3-chlorophosphoenolpyruvate.

0006-2960/96/0435-4349$12.00/0 © 1996 American Chemical Society

Table 1: Intensity Statistics of the Native X-ray Data Set

	shell (Å)										
	total	60−3.88	−3.08	−2.69	−2.44	−2.27	−2.13	−2.03	−1.94	−1.86	−1.80
observations	113340	17941	12518	13361	12352	11365	10639	9957	9416	8563	7200
	71494	7521	7411	7522	7424	7366	7271	7094	7014	6739	6132
independent reflections[a]	(49035)	(7262)	(6786)	(6301)	(5726)	(5350)	(4970)	(4256)	(3558)	(2814)	(2012)
theoretical %	92	96	96	98	97	96	95	93	91	89	81
intensity (av)	4652	10000	9462	5029	3540	3094	2783	2170	1599	1215	905
σ	339	321	414	326	308	322	344	350	346	344	323
R-factor[b] (%)	3.3	2.0	2.5	3.4	4.4	5.2	6.1	7.4	9.6	11.5	13.2

[a] This is the number of reduced observations. Shown in parentheses is the number of independent measurements with $I/\sigma > 3$. [b] $R\text{-factor} = \sum|I - \bar{I}|/\sum I \times 100$.

which binds with higher affinity,[2] metal 1, coordinates to the protein through the carboxylate side chains of Asp 246, Asp 320, and Glu 295 (Lebioda & Stec, 1989). In Mg^{2+}−enolase, three water molecules complete the octahedral coordination shell of metal 1 (Wedekind et al., 1995). The affinity of the weaker binding metal ion, metal 2, is enhanced by binding of substrates or inhibitors. In the complex with the tight binding inhibitor, PhAH [K_i = 15 pM (Anderson et al., 1984)], the carbonyl oxygen and hydroxyl of Ser 39 bind to metal 2 as a chelate to close the active site flap (Wedekind et al., 1994). The presence of two divalent cations in the active site suggests the possibility of electrophilic or electrostatic functions of one or both metal ions in catalysis—especially given the character of the proposed *aci*-carboxylate intermediate. However, interactions of the metal ions with the actual substrates, 2-PGA and P-enolpyruvate, have not been established unambiguously.

There are presently three contrasting views of the catalytic machinery of enolase. These proposals have emerged from separate structural investigations of enolase from yeast (Lebioda & Stec, 1991; Wedekind et al., 1994) and from lobster muscle (Duquerroy et al., 1995). Lebioda and Stec (1991) proposed that metal 1 binds to the C-3-OH of 2-PGA and that the carboxylate side chains of Glu 168 and Glu 211 ionize an intervening water molecule. The resulting OH^- is postulated to serve as the base catalyst in the forward direction. This proposal was, however, based on ambiguous modeling of the electron density corresponding to the carboxylate and hydroxymethyl moieties of the substrate in the active site. Furthermore, only one of the required divalent cations was present in the active site of these crystals (Lebioda & Stec, 1991). An alternative orientation of the substrate was suggested from crystallographic studies of the cocrystallized *bis*-Mg^{2+} complex of yeast enolase and the inhibitor, PhAH (Wedekind et al., 1994). PhAH binds to the enzyme in a bichelate complex with the two divalent metal ions. In this complex, the carbonyl oxygen of PhAH is a μ-bridging ligand (Poyner & Reed, 1992; Wedekind et al., 1994). Because the carbonyl group of PhAH was suggested to mimic the carboxylate of the substrate (Anderson et al., 1984), the stereochemistry of the structure with PhAH implicated Lys 345 as the base catalyst in the forward direction (Wedekind et al., 1994). In contrast, Duquerroy et al. (1995) postulate that a His residue (equivalent to His 159 in yeast enolase) is the base catalyst. The latter proposal was derived from a crystallographic study of lobster enolase in which crystals were soaked with the inhibitor, 2-phosphoglycolate.

The present crystallographic experiments with yeast enolase were initiated in order to determine the binding mode and orientation of 2-PGA and P-enolpyruvate in a cocrystallized complex with both essential divalent cations present in the active site. Crystals of enolase with its equilibrium mixture of 2-PGA and P-enolpyruvate were obtained from solutions of PEG at pH 8. The crystals diffracted to better than 1.8 Å resolution. The present paper reports the molecular structure of this complex.

EXPERIMENTAL PROCEDURES

Crystallization and Data Collection. Enolase was purified from active dry bakers' yeast as described previously (Wedekind et al., 1994). Crystals were grown by the batch method from solutions containing 15 mg mL^{-1} enolase, 15% PEG 8000, 0.25 M KCl, 50 mM HEPPS/KOH, pH 8.0, 2 mM P-enolpyruvate, and 2 mM $MgCl_2$. Microseeding from crystals of enolase−$(Mg^{2+})_2$−PhAH (Wedekind et al., 1994) was used to initiate crystal growth in the first trials. Subsequently, crystallization solutions were seeded with crystals of the target complex. Crystals of the substrate/product complex belong to the space group *C*2 and have one dimer per asymmetric unit. Unit cell dimensions are a = 121.9 Å, b = 73.2 Å, c = 93.9 Å, and β = 93.3°. The crystals are isomorphous with those of enolase−$(Mg^{2+})_2$−PhAH (Wedekind et al., 1994). X-ray data were collected with a Siemens HI-STAR dual detector mounted on a Rigaku rotating anode operated at 50 kV, 80 mA, and a 300 μm focal spot. The X-ray beam was collimated by double focusing mirrors. The crystal to detector distances were 15.0 and 24.2 cm for the high- and low-resolution detectors, respectively. X-ray data were obtained in the 512 × 512 pixel format, processed with the program XDS (Kabsch, 1988a,b) and scaled using the program Xscalibre (G. Wesenberg and I. Rayment, unpublished results). The data set was 92% complete to 1.8 Å with an overall merging *R*-factor of 3.3% (Table 1).

X-ray data were collected on one crystal (0.2 × 0.5 × 1.3 mm^3) that was flash cooled to −160 °C. The procedures used for crystal mounting and freezing are described by Teng (1990) and Rodgers (1994). Prior to freezing, the crystal was equilibrated with the cryoprotectant, ethylene glycol.

[2] In much of the previous literature concerning enolase, the metal ion which binds with higher affinity to enolase has been called the conformational metal ion and the metal ion which binds with lower affinity has been called the catalytic metal ion. In light of previous structural data on the intermediate analog, PhAH (Poyner & Reed, 1992; Wedekind et al., 1994), and the present data which show that both metal ions bind directly to the substrate, the metal ions will be labeled metal 1 and metal 2, respectively, and their binding sites will be called site 1and site 2, respectively.

This equilibration was carried out by serial transfers of the crystal to solutions containing increasing concentrations of ethylene glycol. All crystal transfer solutions contained 50 mM HEPPS/KOH, pH 8.0, 20% PEG 8000, 2 mM P-enolpyruvate, and 2 mM $MgCl_2$ (solution A). The crystal was first moved from the mother liquor to solution A containing 0.25 M KCl and allowed to equilibrate for 5 min. Then the crystal was moved to solution A having 10% ethylene glycol and 0.33 M KCl and equilibrated for 2 min. The crystal was transferred two additional times, first to solution A plus 15% ethylene glycol and 0.33 M KCl for 2 min and then to solution A plus 17% ethylene glycol and 0.33 M KCl solution. The crystal was flash frozen within ~30 s after being moved into this final transfer solution.

Refinement. Initial phases were calculated from the refined coordinates of the PhAH structure leaving out PhAH, metal ions, and water molecules. The initial *R*-factor was 39.6% for all data to 1.8 Å. Crystallographic least-squares refinement of the model by the program TNT (Tronrud et al., 1987) reduced the *R*-factor to 30% for all data to 1.8 Å. Manual adjustments in the model were then made with the programs FRODO (Jones, 1985) and O (Jones et al., 1991). Density corresponding to the magnesium ions and substrate/product was clearly present in the initial, unrefined electron density maps; however, the substrate/product and magnesium ions were included in the model at this intermediate stage of refinement. After further refinement, water molecules were added to the model. The peak searching algorithm in the TNT package was used to locate positions of ordered water molecules. Following completion of manual adjustments and inclusion of all waters, the model was refined excluding P-enolpyruvate and 2-PGA. The resulting ($F_o - F_c$) electron density map provided a view of the combined density of substrate and product. 2-PGA and P-enolpyruvate were each assigned occupancies of 0.5, consistent with the internal equilibrium constant (Burbaum & Knowles, 1989), and returned to the model for a final round of least-squares refinement. The current *R*-factor for all data to 1.8 Å is 17.7%. The present dimeric model includes 942 water molecules (temperature factors <65). The rms deviations from the target geometries are 0.018 Å for bond lengths, 2.1° for bond angles, and 0.009 Å for coplanar groups. The coordinate error for the model is estimated to be 0.175 Å on the basis of a Luzzati plot (not shown) (Luzzati, 1952). A Ramachandran plot for the dimer main-chain non-glycinyl dihedral angles is shown in Figure 1.

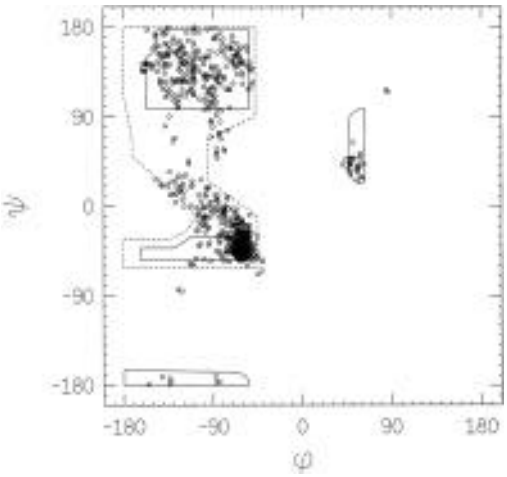

FIGURE 1: Ramachandran plot of dimeric yeast enolase main-chain non-glycinyl dihedral angles. Fully allowed φ and ψ values are shown by solid enclosures. Partially allowed regions are enclosed by broken lines. Dihedral angles for the most severe outliers are distorted by hydrogen-bonding and ionic interactions. The most severe left-handed helical outlier in both subunits is Arg 402, whose guanidinium group interacts with Glu 404. The most severe right-handed outlier in both subunits is Asp 320, which interacts with Mg^{2+} I.

Table 2: Disordered Side Chains[a]

amino acid subunit I	disordered atoms	amino acid subunit II	disordered atoms
Lys 4	ζ		
Lys 53	δ, ϵ, ζ	Lys 53	δ, ϵ, ζ
Lys 66	δ, ϵ, ζ	Asn 80	Oδ1
Lys 78	ϵ, ζ	Lys 87	δ, ϵ, ζ
Lys 87	δ, ϵ, ζ	Lys 104	ϵ, ζ
Lys 131	ϵ, ζ	Lys 138	ϵ, ζ
Lys 140	ζ	Lys 140	ϵ, ζ
Ser 142	Oγ	Ser 142	Oγ
Lys 177	δ, ϵ, ζ	Lys 177	δ, ϵ, ζ
Lys 199	ϵ, ζ	Lys 199	ϵ, ζ
Gln 219	Cγ, Cδ, Oϵ1, Nϵ2	Gln 219	Nϵ2
Lys 240	ζ	Lys 240	δ, ϵ, ζ
Lys 257	ζ	Lys 269	δ, ϵ, ζ
Lys 287	γ, δ, ϵ, ζ	Lys 271	γ, δ, ϵ, ζ
Glu 304	Cδ, Oϵ1, Oϵ2	Glu 304	Cγ, Cδ, Oϵ1, Oϵ2
Lys 311	ϵ, ζ	Lys 311	δ, ϵ, ζ
Lys 328	δ, ϵ, ζ	Lys 328	δ, ϵ, ζ
Lys 337	ϵ, ζ	Glu 335	Oϵ1, Oϵ2
Asp 421	Cγ	Lys 337	ϵ, ζ
Asn 422	Nδ2		

[a] Atoms have negligible electron density $>1.0\sigma$ and $B \geq 95$ Å^2.

RESULTS AND DISCUSSION

Figure 2 illustrates representative electron density calculated from the coefficients ($2F_o - F_c$). All residues in each subunit have well-defined side chains except those of some surface residues listed in Table 2. The overall chain topology of the equilibrium mixture of enolase is identical to that described previously for yeast enolase (Stec & Lebioda, 1990; Wedekind et al., 1994). The region, extending from Gly 37 through His 43, of the active site loop exhibits the same conformation as that found in the complex of PhAH by Wedekind et al. (1994) as does the loop containing His 159. Ser 39, in the center of the active site loop, chelates to the site 2 magnesium to seal off the active site in a manner identical to that revealed in the structure with PhAH. The overall rms displacement of α-carbons of the dimer in the structure of the substrate/product relative to that of PhAH is 0.32 Å. The α-carbons of the monomers superimpose with rms displacements of 0.27 Å.

Substrate/Product Electron Density. Difference ($F_o - F_c$) electron density of the substrate/product is shown in Figure 3. The difference density of Figure 3 was generated by excluding 2-PGA and P-enolpyruvate from the refinement and phase calculation. The density exhibits well-defined lobes for the phosphate and carboxylate oxygens of the substrate/product which immediately defines the stereochemistry of substrate/product binding. Strong density representing the hydroxymethyl of 2-PGA (and C-3 of P-enolpyruvate) extends outward toward the carboxyl side chain of Glu 211. A ball-and-stick model of 2-PGA is shown in the density. P-enolpyruvate (not shown) also fits well into the observed electron density except for the extra density corresponding to the C-3-OH of 2-PGA. The fact that density corresponding to the substrate/product is confined

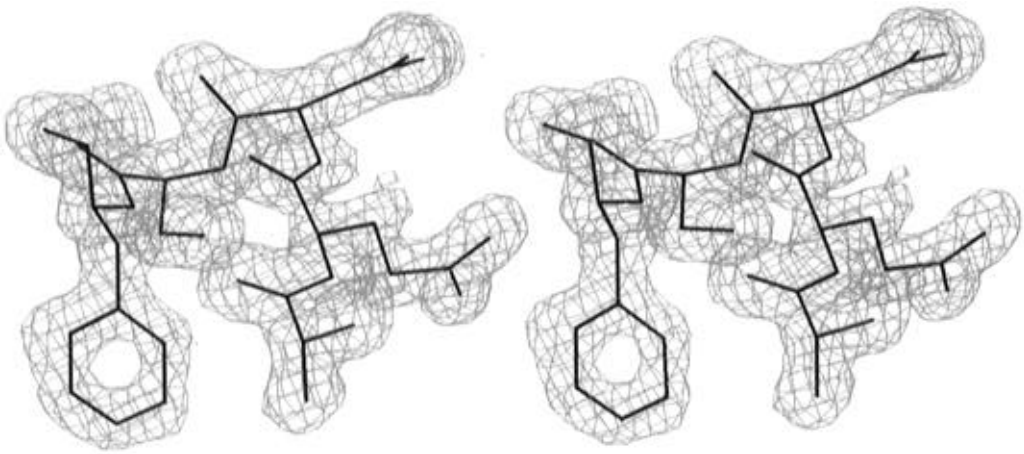

FIGURE 2: Representative portion of the ($2F_o - F_c$) electron density map calculated with the final refined phases. Electron density for residues ^{359}AQDSF of subunit II is contoured at 1.2σ. The program MOLVIEW (Smith, 1990) was used to prepare this figure and Figures 3 and 5.

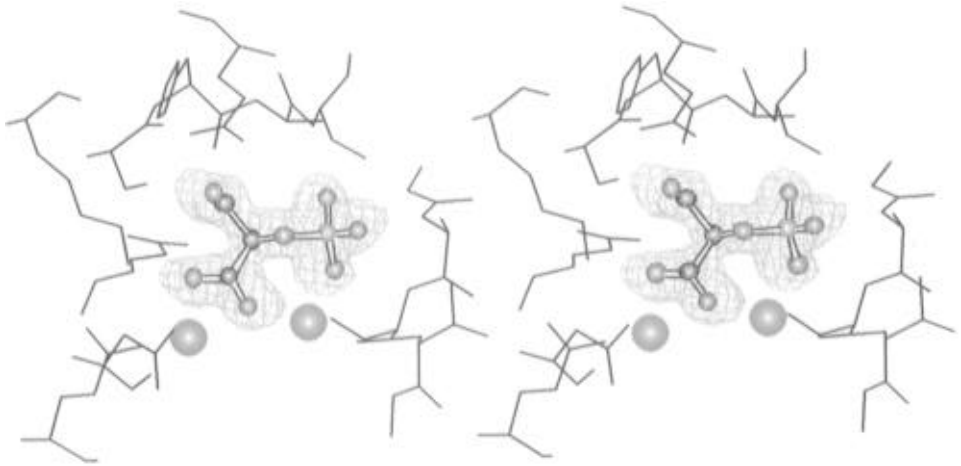

FIGURE 3: ($F_o - F_c$) electron density map contoured at 3σ for the substrate/product in subunit II. A ball-and-stick model of 2-PGA is shown in the density. The magnesium ions and some of the surrounding side chains are also shown. Color codes: green, Mg^{2+}; gray, carbon; red, oxygen; blue, nitrogen; purple, phosphorus.

to the overall shape of 2-PGA (or P-enolpyruvate) indicates there is no appreciable shift in the position of the substrate skeleton upon the transformation of substrate to product. Moreover, side chains of amino acid residues in the active site are well defined in their densities (not shown), indicating that the interconversion of substrate and product has minimal influences on the structure within the cavity of the active site. Adjustments in protein conformation appear to be relegated to loop movements which are completed when the Ser 39 of the active site loop chelates to Mg^{2+} 2 (Wedekind et al., 1994).

The density for the C-3-OH of 2-PGA is not diffuse in the maps (Figure 3) because the enzymatic reaction is quenched at −160 °C. Hence, interconversion of substrate and product does not take place during data collection, and occupancies consistent with the enzyme equilibrium (Burbaum & Knowles, 1989) reflect this situation. Whereas strong density appears for the C-3-OH of 2-PGA in the difference map of Figure 3, a difference map (not shown) calculated with 2-PGA and P-enolpyruvate included in the refinement and phase calculation does not reveal density that could be construed as the substrate water molecule. The location of the substrate water molecule in serine proteases has proven to be somewhat contentious (Singer et al., 1993a,b; Perona et al., 1993). At this point, the known stereochemistry of the reaction (Cohn et al., 1970) provides the direction of attack of the substrate water, and evidence from mutagenesis (Poyner et al., 1996) indicates that Glu 211 is likely involved in its activation.

Coordination of Magnesium Ions. Coordination schemes of the two magnesium ions are illustrated in Figure 4. Metal 1 coordinates to carboxylate oxygens from the side chains of Asp 246, Glu 295, and Asp 320 as observed in all previous structures of metalloenolase (Lebioda & Stec, 1989, 1991; Lebioda et al., 1993; Wedekind et al., 1994, 1995; Duquerroy et al., 1995). The hexacoordinate ligand sphere of metal 1 is completed by a bidentate coordination to the carboxylate of the substrate/product and coordination of a single water molecule. Bidentate coordination of carboxylates to Mg^{2+} is not a common motif; however, the $Mg^{2+}-O$ bond distances (2.3−2.4 Å) of the bidentate carboxylate group fall into the range where bidentate coordination is prevalent with other divalent cations (Carrell et al., 1988). One of the carboxylate oxygens is also liganded to metal 2. This carboxylate oxygen is thus a μ-bridging ligand for the two magnesium ions and is therefore structurally analogous to the carbonyl oxygen of PhAH. The Cambridge Structural Data Base contains several entries of divalent metal complexes having a bidentate carboxylate to one metal ion and one O as a μ-carboxylato bridge to a second metal ion. The

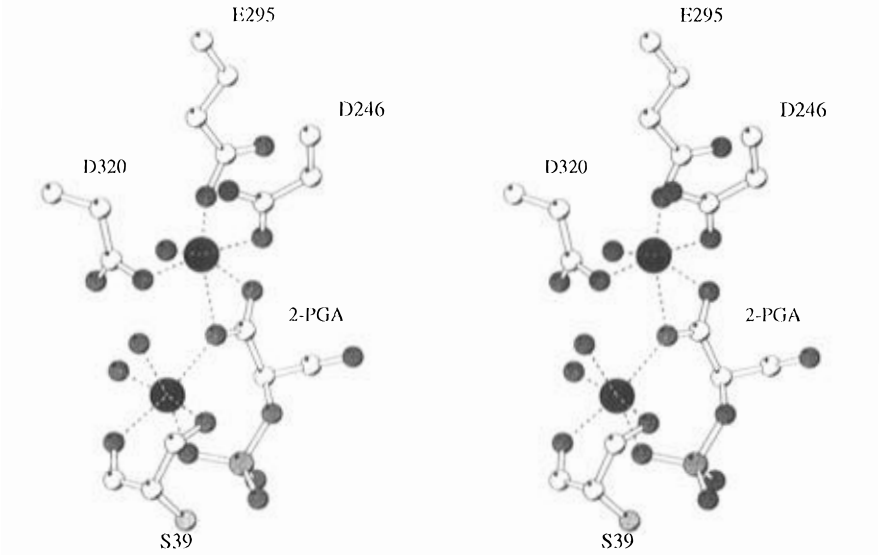

FIGURE 4: Stereoview of the coordination of the two magnesium ions in the enolase−$(Mg^{2+})_2$−2-PGA complex. The black spheres represent the magnesium ions. The unlabeled spheres represent waters. The dashed lines show the coordination for the magnesium ions. The program MOLSCRIPT (Kraulis, 1991) was used to prepare this figure and Figures 6, 7, and 8.

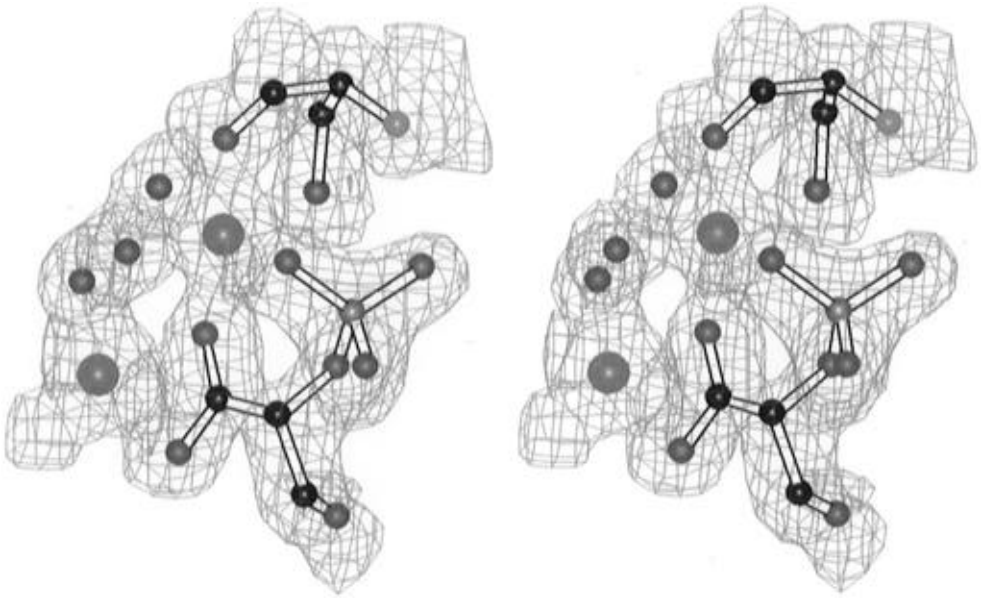

FIGURE 5: $(2F_o - F_c)$ electron density map contoured at 1σ and calculated with the final refined phases. The magnesium ions, the substrate/product, Ser 39, and three water molecules of subunit I are shown. 2-PGA has been modeled in for the substrate/product density. Ser 39 is directly above Mg^{2+} II. The complete coordination of Mg^{2+} II is shown. For Mg^{2+} I, for clarity, only the carboxylate ligands of 2-PGA and a water ligand are shown.

Scheme 2

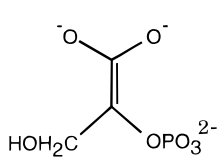

aci carboxylate intermediate

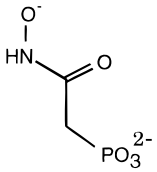

PhAH trianion

carbonyl oxygen and −NH−O⁻ moieties of PhAH were originally suspected of mimicking the carboxylate and hydroxymethyl moieties of the intermediate, respectively (Anderson et al., 1984; Poyner & Reed, 1992; Wedekind et al., 1994). It is now clear, however, that the entire hydroxamate moiety of PhAH mimics just the carboxylate of the substrate/product (Scheme 2).

The substrate/product chelates to metal 2 through the μ-bridging oxygen of the carboxylate and an oxygen from the phosphate group. The other four ligands of this second Mg^{2+} are the carbonyl and γ-oxygens of Ser 39 and two water molecules (Figure 4). As indicated by the electron density in Figure 5, the position and coordination scheme of each Mg^{2+} are unambiguous. The intricate flap closure mechanism—chelation of Ser 39 to the site 2 Mg^{2+}—observed in the complex with PhAH (Wedekind et al., 1994) reinforced the notion that metal 2 was in the "natural" position in the PhAH structure. Observation of this same Ser 39−Mg^{2+} chelate interaction in the present structure confirms this supposition. The two metals are separated by ~4.2 Å.

Coordination of the carboxylate moiety of the substrate/product to both magnesium ions in the active site of enolase suggests that the first step of the reaction—ionization of 2-PGA to give the *aci*-carboxylate intermediate—and stabi-

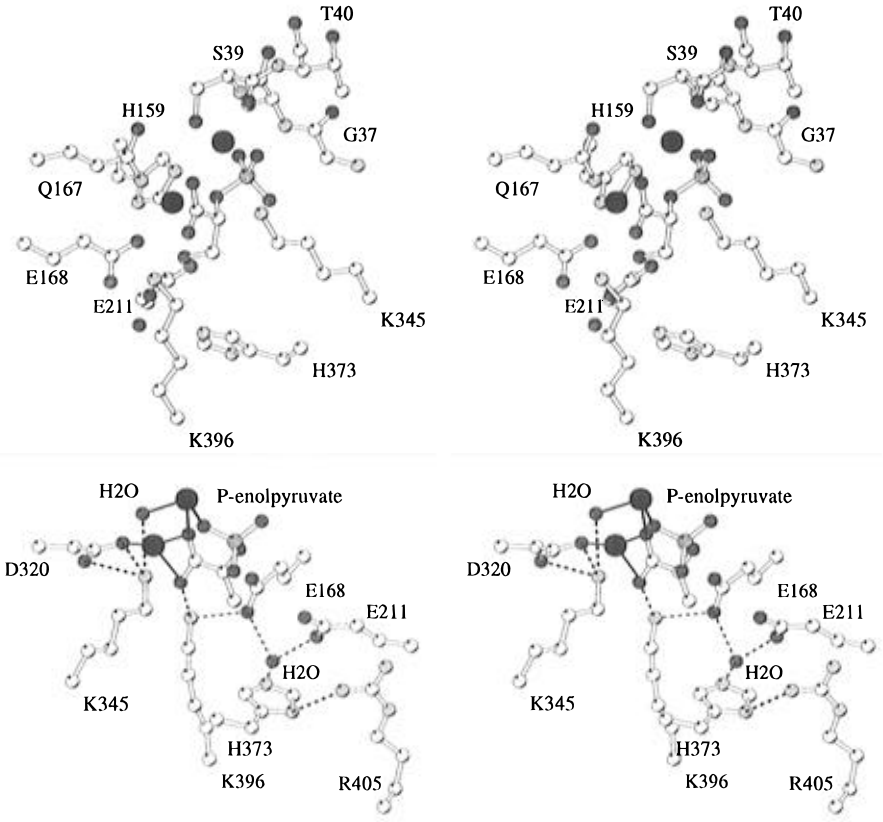

FIGURE 6: (a, top) Stereoview of the active site of the enolase−$(Mg^{2+})_2$−2-PGA complex in subunit I. The two large black spheres are the magnesium ions. The ball-and-stick model of 2-PGA is shown in gray. A water molecule between Glu 211 and Glu 168 is shown as a small black sphere. For simplicity, water ligands were not included. (b, bottom) Stereoview of the potential H-bonding network in the active site enolase−$(Mg^{2+})_2$−2-P-enolpyruvate complex in subunit I. The large black spheres are the magnesium ions. The dashed lines represent interaction distances of <2.94 Å.

lization of the intermediate are promoted by this coordination scheme. Furthermore, it is evident that both metal ions participate in this crucial aspect of enolase catalysis. Metal coordination enhances the rate of solvent ^1H or ^2H exchange into methylene groups which are adjacent to metal-coordinated carboxylates in chelates of EDTA and related complexing agents (Williams & Busch, 1965; Terrill & Reilley, 1966). This same metal ion-promoted solvent exchange is also observed in methylene groups adjacent to carboxylates in peptide complexes with metal ions (Gillard et al., 1968). These model reactions provide perhaps the closest precedent for the first step in catalysis by enolase.

Stereochemistry of the Active Site. The strong electron density of the substrate/product (Figure 3) clearly defines the positions of the phosphate, carboxylate, and hydroxymethyl groups of 2-PGA. The view of the active site given in Figure 6a shows that the ϵ-amino group of Lys 345 is in position to function as the base in removal of the proton at C-2 of 2-PGA. Furthermore, the ϵ-amino of Lys 345 is the only basic functional group accessible to this proton. Rose and co-workers (Cohn et al., 1970) determined that the enolase-catalyzed elimination of water from 2-PGA has *anti* stereochemistry. Hence, any groups assisting in the leaving ability of the C-3-OH in the forward direction or in activation of water for attack in the reverse reaction should be found on the side of the substrate opposite to Lys 345. The carboxyl side chain of Glu 211 fits this pattern—being on the side opposite to Lys 345 and proximate to the hydroxymethyl group of 2-PGA. The side chain of His 373 is, however, also close to the hydroxymethyl group, and the carboxyl of Glu 168 is near that of Glu 211. The positions of these side chains suggest the possibility that either the carboxyl of Glu 211 or the imidazole of His 373 serves as such an acid/base catalyst in the second step of the forward reaction and in activation of water for attack at C-3 of P-enolpyruvate in the reverse reaction. Potential H-bonding interactions (distances <2.95 Å) among active site residues including ordered water molecules are shown in Figure 6b.

The extra negative charge on the putative *aci*-carboxylate intermediate is located on the carboxylate oxygens (Anderson et al., 1984). As noted above, the structure indicates that both metal ions are recruited to stabilize this charge redistribution. The effective charge of metal 1 is, however, attenuated by the three carboxylate ligands from the protein. The ϵ-amino group of Lys 396 is within H-bonding distance of a carboxylate oxygen (the oxygen that is not the μ-ligand) of the substrate/product. An interaction of the carboxylate oxygen with a protonated ϵ-amino group of Lys 396 appears a likely additional source of charge stabilization for the intermediate. The carboxyl of Glu 168, proximate to the ϵ-amino of Lys 396 as well as to the carboxyl of Glu 211, may be essential for proper orientation of these groups. The carboxyl of Glu 168 would also influence the pK_a's of Glu 211 and Lys 396. Hence, Glu 168 is essential in the overall reaction as indicated by site-directed mutagenesis results with E168Q enolase (Brewer et al., 1993; Poyner et al., 1996).

A single water molecule is positioned between Glu 211, Glu 168, and His 373 (Figure 6). This water molecule is structurally analogous to the water postulated to function as the catalytic base in the scheme proposed by Lebioda and Stec (1991). However, this water is >6 Å from C-2 of the substrate and on the wrong side of the substrate to be

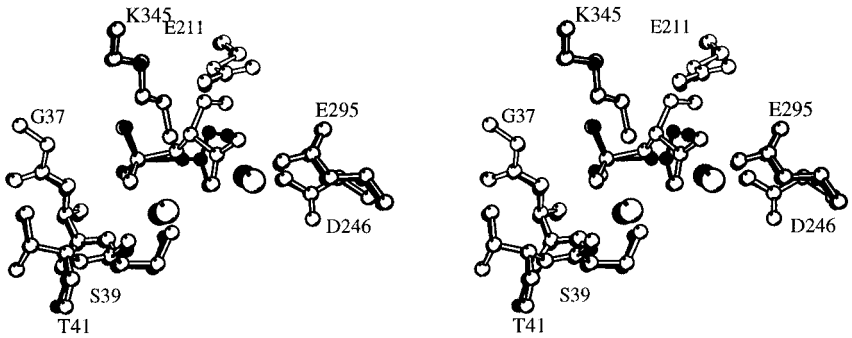

FIGURE 7: Stereoview of the subunit I active site of the enolase−$(Mg^{2+})_2$−2-PGA complex shown in open lines. The solid lines represent superimposed residues of the enolase−$(Mg^{2+})_2$−PhAH complex (Wedekind et al., 1994). Water molecules are not included.

involved as the base catalyst.

Correlations with Results from Site-Directed Mutagenesis. Three of the active site residues discussed above, Glu 168, Glu 211, and Lys 345, have been changed to other residues through site-directed mutagenesis. Thus, Brewer, Lebioda, and co-workers (Brewer et al., 1993; Sangadala et al., 1995) have constructed genes corresponding to E168Q and E211Q enolase and expressed and purified these mutant proteins in yeast. Both mutant proteins exhibited severely depressed activities in the overall reaction, but both proteins were functional, at reduced rates, in the ionization of the inhibitor, TSP. Poyner et al. (1996) overexpressed the genes corresponding to E168Q, E211Q, and K345A enolase in *Escherichia coli* and isolated the mutant proteins. The abilities of the mutant enzymes to carry out the first step in the reaction were assayed by the exchange of the C-2 proton of 2-PGA with deuterons in solutions of D_2O. Both E168Q and E211Q enolases catalyzed this $^1H/^2H$ exchange—E211Q enolase being nearly as effective as wild-type enolase. However, K345A enolase was inactive in this $^1H/^2H$ exchange reaction. Furthermore, K345A enolase did not catalyze ionization of bound TSP. These observations were consistent with the absence of the base catalyst in the K345A protein, whereas the data show that an effective base is present in E168Q and E211Q enolases.

The altered rates of ionization of TSP catalyzed by E168Q and E211Q enolase have been interpreted (Brewer et al., 1993; Sangadala et al., 1995) as being consistent with the general base catalysis scheme proposed by Lebioda and Stec (1991) wherein Glu 211 and Glu 168 ionize an intervening water molecule. The facile catalysis of the $^1H/^2H$ exchange of 2-PGA by E211Q and E168Q enolase (Poyner et al., 1996) is, however, incompatible with the mechanism proposed by Lebioda and Stec (1991). Both of these Glu to Gln mutant proteins remain competent in the first step of the reaction—ionization of 2-PGA. On the other hand, the results with K345A enolase are fully consistent with the present structure, which shows that the C-2 proton of 2-PGA is directed toward the ϵ-amino group of Lys 345. Furthermore, the crystallographic results presented here, as well as results from the K345A mutant protein, contradict the suggestion of Duquerroy et al. (1995) that His 159 (yeast enolase numbering system) is the catalytic base.

Poyner et al. (1996) also determined the capacity of the three mutant forms of enolase to catalyze the hydrolysis of *(Z)*-3-Cl-P-enolpyruvate. This reaction is analogous to the reverse reaction of enolase in that the enzyme activates a water molecule for attack at C-3 of the substrate. The order of activities in catalysis of this reaction—wild type > K345A > E168Q ≫ E211Q—suggested that Glu 211 was possibly involved in activation of the attacking water molecule. This interpretation is also fully consistent with the present structure, which reveals that Glu 211 interacts with the C-3-OH of 2-PGA.

Comparison of Equilibrium Mixture and PhAH Structures. Of all the reported structures of enolase, the complex of the substrate/product bears the greatest resemblance to that of enolase−$(Mg^{2+})_2$−PhAH (Wedekind et al., 1994). Figure 7 shows the region of the active site resulting from a superposition of the coordinates of the two structures. Figure 7 reveals that the complex with PhAH maintains the two metal ions and side chains of active site residues in virtually the same locations as they occur in the complex of the substrate/product mixture. The active site loop containing Ser 39 and the flexible loop containing His 159 undergo movement to virtually the same positions in the substrate/product and PhAH complexes.

As noted above, the entire $-C(O)-NHO^-$ of PhAH substitutes for the carboxylate of the substrate/product. The strong chelating ability of the hydroxamate moiety, relative to that of a carboxylate group, enhances binding of PhAH, over that of substrate/product, to metal 1. It is now apparent, however, that PhAH lacks a surrogate of the hydroxymethyl group of the authentic reaction intermediate and that, barring some as yet undisclosed ionization, PhAH does not have an sp^2 hybridized carbon at a position analogous to C-2 of the substrate. Hence, PhAH does not fit into the category of "intermediate state" analog—at least by the criterion of sp^2 hybridization at C-2 (Anderson et al., 1984). On the other hand, the present structure shows that charge redistribution in the intermediate is stabilized by the magnesium ions and by a protonated ϵ-amino of Lys 396. In the sense that the extra negative charge on the *aci*-carboxylate intermediate intensifies interaction with these cations, the strong interaction of the hydroxamate of PhAH with both magnesium ions as well as with the ϵ-ammonium of Lys 396 does mimic this property of the intermediate.

As noted by Poyner and Reed (1992), PhAH forms two favorable (one five- and one six-membered) chelate rings in its interaction with the two metal ions in the active site of enolase. Metal 2 is seized by the six-membered chelate ring of PhAH with a higher affinity than by the seven-membered ring present in the substrate/product complex. Thus, metal 2 binds tighter to the complex with PhAH than to the substrate/product complex. This situation probably stiffens the "latch" provided by chelation of Ser 39 (in the active site flap) to metal 2. Such favorable chelate interactions, together with the "snug fit" of the phosphonate moiety in

the pocket anchored by the side chain of Arg 374, likely account for the exceptional stability of the PhAH complex.

Perspectives on Contrasting Proposals for Catalytic Machinery of Enolase. The active site of enolase is lined with acidic, basic, and polar residues. Hence, there is no shortage of candidates for acid/base catalysts. Therefore, precise knowledge of the stereochemistry of substrate and metal cofactor binding is essential for proper identification of these groups. Moreover, enzymatic activity of enolase requires the presence of two divalent cations per active site (Faller et al., 1977). Structures on which competing proposals of the enolase mechanism are based (Lebioda & Stec, 1991; Duquerroy et al., 1995) lacked the second essential divalent cation.

Problems encoutered in locating metal 2 in several previous crystallographic studies of enolase (Lebioda & Stec, 1991; Zhang et al., 1994b; Duquerroy et al., 1995) can be attributed to the use of concentrated $(NH_4)_2SO_4$ to promote crystallization. The use of high concentrations of $(NH_4)_2SO_4$ to promote crystallization is problematic in studies of enzymes such as enolase which bind one or more metal cofactors with moderate affinity. The dissociation constants of complexes between SO_4^{2-} and, for example, Mg^{2+} and Mn^{2+} are ~5 mM (Sillén & Martell, 1964). Concentrations of SO_4^{2-} in excess of 2 M are commonly used in crystallization (Lebioda & Stec, 1991; Zhang et al., 1994b; Duquerroy et al., 1995), and the excess SO_4^{2-} buffers free metal ion at too low a concentration to allow sufficient population of weaker affinity metal sites for structural analysis. The use of lithium salts as precipitants (Zhang et al., 1994a) is similarly problematic, because Li^+ inhibits enolase competitively with respect to Mg^{2+} (Kornblatt & Musil, 1990). Furthermore, Li^+, occupying a Mg^{2+} site, might go undetected because Li^+ has only two electrons to scatter X-rays. In lieu of such salts, nonionic precipitants, such as PEG, appear to be superior in crystallization of enolase and other enzymes which bind metals with moderate affinity.

Wedekind et al. (1994) observed significant changes in the positions of loops and movements in the C-terminal domain that were apparent when the structure of the cocrystallized complex with PhAH was superimposed on that of the apoenzyme (Stec & Lebioda, 1990). Although some of these changes might occur in the confines of a protein crystal, cocrystallization of the target complexes would seem to be preferred over soaking as the conservative approach to introduction of substrates, metal cofactors, and inhibitors into the active site of enolase.

Different ideas about the placement and orientation of the substrate in the active site of enolase have naturally led to differences in the assignment of catalytic groups and their respective roles in catalysis (Lebioda & Stec, 1991; Wedekind et al., 1994; Duquerroy et al., 1995). In their study of the equilibrium mixture, Lebioda and Stec (1991) soaked crystals of Mg^{2+}−enolase in 3 M $(NH_4)_2SO_4$ at pH 6 with substrate. These workers noted, however, that density for the substrate/product was ambiguous with respect to placement of the carboxylate and hydroxymethyl groups. The high concentration of SO_4^{2-} also precluded binding of the second equivalent of Mg^{2+}. The conformer having the hydroxymethyl group oriented toward site 1 Mg^{2+} (which places the proton at C-2 under the influences of Glu 168 and Glu 211) was chosen for mechanistic discussions by Lebioda and Stec (1991). Wedekind et al. (1994) suggested that Lys 345 could not be ruled out as the base given the ambiguity noted above and a presumed correspondence between the carbonyl group of PhAH and the carboxylate of the substrate/product. The electron density of the substrate/product given in Figure 3 clearly shows that it is the carboxylate—not the hydroxymethyl—of the substrate which interacts with metal 1. Furthermore, the present structure establishes that the ϵ-amino group of Lys 345 is the only functional group near the C-2 proton of 2-PGA.

Suggestions regarding the position of substrate binding and the mechanism of enolase proposed by Duquerroy et al. (1995) were based on data obtained from soaking crystals of lobster enolase with the weak inhibitor, 2-phosphoglycolate. These experiments were conducted in a background of 2.5−2.7 M $(NH_4)_2SO_4$, and it is, therefore, not surprising that only one divalent metal ion was found in the active site. Lebioda et al. (1991) reported the structure of 2-phosphoglycolate bound to Zn^{2+}−enolase under similar salt conditions. The structure of the Zn^{2+} complex, however, showed that the carboxylate of the inhibitor coordinated to the metal ion. This carboxylate−metal ion coordination was not apparent from density assigned to the inhibitor in crystals of the lobster enzyme. Duquerroy et al. (1995) advocate coordination of the hydroxymethyl group—absent in their structure of 2-phosphoglycolate—to metal 1 and cite a "preponderance of biochemical evidence" as support for this suggestion. The evidence cited is, however, necessarily indirect. The present structure of the authentic substrate/product complex clearly shows that the C-3-OH is not coordinated to metal 1. Furthermore, Nϵ2 of His 159 (yeast enolase numbering system), which was nominated by Duquerroy et al. (1995) to be the catalytic base, interacts with a peripheral oxygen of the phosphate group and is situated on the wrong side of 2-PGA to function as the catalytic base.

There has also been contention regarding the position of metal 2 in the active site (Poyner & Reed, 1992; Lee & Nowak, 1992; Zhang et al., 1994b; Wedekind et al. 1994; Duquerroy et al., 1995). In this regard, it is noteworthy that studies of the enolase complex with PhAH appear to be the only previous structural studies wherein the stoichiometry and composition of the two metal ions per active site were clearly defined (Poyner & Reed, 1992; Wedekind et al., 1994). Zhang et al. (1994b) soaked PhAH and Mn^{2+} into a crystal of apoenolase at pH 6 in 3 M $(NH_4)_2SO_4$. After modeling in PhAH, the authors interpreted their difference electron density as the second Mn^{2+}, bound in a bidentate fashion to the phosphonate oxygens of the inhibitor and to the carbonyl oxygen of Gly 37 (the hinge residue of the active site loop). However, this Mn^{2+} coordination was inconsistent with that of site 2 determined by Mn^{2+} EPR measurements using ^{17}O-labeled PhAH (Poyner & Reed, 1992). In addition, the interpretations of Zhang et al. (1994b) were incompatible with the unambiguous ($F_o - F_c$) density of the inhibitor and metal 2 obtained from cocrystals of the enolase−$(Mg^{2+})_2$−PhAH complex prepared at pH 8 in a lower salt background (Wedekind et al., 1994).

Enolase binds divalent metal ions at ancillary sites in the presence of high concentrations of divalent metal ion (Faller et al., 1977). Crystals used in the present study were obtained from solutions of 2 mM Mg^{2+}—a concentration that approximates the optimum concentration of Mg^{2+} in assays of enolase activity. Hence, this site has all the structural

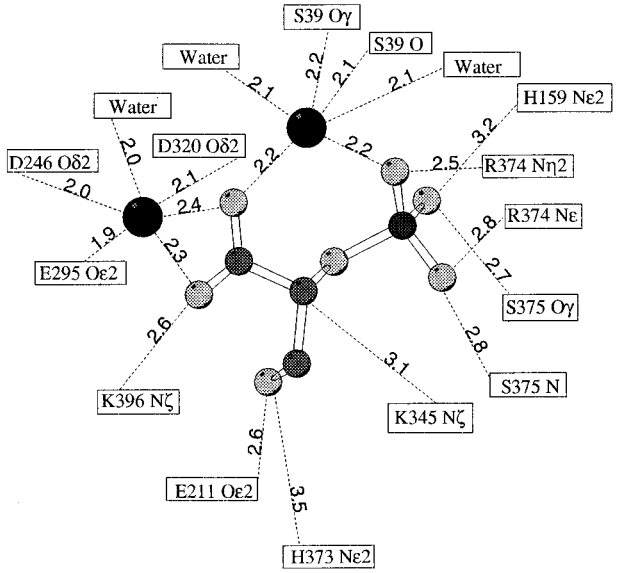

FIGURE 8: Schematic diagram of the enolase active site residue interactions with the $(Mg^{2+})_2$−substrate/product complex. The dashed lines from 2-PGA to amino acids represent possible hydrogen bonds. The dashed lines from the magnesium ions indicate their coordination. Interatomic distances in angstroms are given on the dashed lines.

and functional characteristics of the activation site, site 2, of enolase. Again, the present structural data confirm the conclusions regarding the position and liganding of metal 2 derived from the studies with PhAH (Poyner & Reed, 1992; Wedekind et al., 1994).

Conclusions. Major contacts of 2-PGA with divalent metal ions and active site residues in enolase are summarized in Figure 8. Both essential divalent cations interact with the carboxylate of the substrate/product and, by inference, with the *aci*-carboxylate moiety of the intermediate. The structure provides a logical rationale for two fundamental enzymological characteristics of enolase: (1) the synergy in binding of substrates and metal 2; and (2) the catalytic requirement for two divalent cations.

The ϵ-amino of Lys 396 is in a position to H-bond to one of the carboxylate oxygens of the substrate/product. The divalent cations, together with the ϵ-ammonium moiety of Lys 396, are situated to promote and stabilize the redistribution of negative charge that occurs in formation of the *aci*-carboxylate intermediate. The binuclear metal center and the ϵ-ammonium moiety of Lys 396 clearly function as the enolization catalysts.

The ϵ-amino group of Lys 345 is the only viable candidate for the active site base, which accepts a proton from C-2 of 2-PGA in the first step of the reaction. The structure is consistent with the failure of K345A enolase to catalyze $^1H/^2H$ exchange in 2-PGA (Poyner et al., 1996). The carboxyl side chain of Glu 211 is proximate to the C-3-OH of 2-PGA, and either this carboxyl or the side chain of His 373 is in position to serve as acid catalysts in the second step of the reaction. The importance of Glu 211 in the second step of the reaction was also uncovered in studies of E211Q enolase catalysis of the hydration of (*Z*)-3-Cl-P-enolpyruvate (Poyner et al., 1995). The locations of Lys 345 and Glu 211 are fully consistent with the *anti* stereochemistry of the elimination reaction (Cohn et al., 1970).

ACKNOWLEDGMENT

We are grateful to Dr. James Thoden for assistance with data collection and to Dr. Russell Poyner for purified yeast enolase and helpful discussions.

REFERENCES

Anderson, S. R., Anderson, V. E., & Knowles, J. R. (1994) *Biochemistry 33,* 10545−10555.

Anderson, V. E., Weiss, P. M., & Cleland, W. W. (1984) *Biochemistry 23,* 10498−10503.

Babbitt, P. C., Mrachko, G. T., Hasson, M. S., Huisman, G. W., Kolter, R., Ringe, D., Petsko, G. A., Kenyon, G. L., & Gerlt, J. A. (1995) *Science 267,* 1159−1161.

Brewer, J. M., Robson, R., Glover, C. V. C., Holland, M. J., & Lebioda, L. (1993) *Proteins: Struct., Funct., Genet. 17,* 426−434.

Burbaum, J. J., & Knowles, J. R. (1989) *Biochemistry 28,* 9306−9317.

Carrell, C. J., Carrell, H. L., Erlebacher, J., & Glusker, J. P. (1988) *J. Am. Chem. Soc. 110,* 8651−8656.

Cohn, M., Pearson, J. E., O'Connell, E. L., & Rose, I. A. (1970) *J. Am. Chem. Soc. 92,* 4095−4098.

Dinovo, E. C., & Boyer, P. D. (1971) *J. Biol. Chem. 246,* 4586−4593.

Duquerroy, S., Camus, C., & Janin, J. (1995) *Biochemistry 34,* 12513−12523.

Faller, L. D., Baroudy, B. M., Johnson, A. M., & Ewall, R. X. (1977) *Biochemistry 16,* 3864−3869.

Gerlt, J. A., & Gassman, P. G. (1992) *J. Am. Chem. Soc. 114,* 5928−5934.

Gerlt, J. A., & Gassman, P. G. (1993) *J. Am. Chem. Soc. 115,* 11552−11568.

Gillard, R. D., Mitchell, P. R., & Payne, N. C. (1968) *Chem. Commun.,* 1150−1151.

Guthrie, J. P., & Kluger, R. (1993) *J. Am. Chem. Soc. 115,* 11569−11572.

Jones, T. A. (1985) *Methods Enzymol. 115,* 157−171.

Jones, T. A., Zou, J. Y., Cowan, S. W., & Kjeldgaard, M. (1991) *Acta Crystallogr. A47,* 110−119.

Kabsch, W. (1978) *Acta Crystallogr., Sect. A 32,* 922−923.

Kabsch, W. (1988a) *J. Appl. Crystallogr. 21,* 67−71.

Kabsch, W. (1988b) *J. Appl. Crystallogr. 21,* 916−924.

Kornblatt, J. M., & Musil, R. (1990) *Arch. Biochem. Biophys. 277,* 301−305.

Kraulis, P. J. (1991) *J. Appl. Crystallogr. 24,* 946−950.

Lebioda, L., & Stec, B. (1989) *J. Am. Chem. Soc. 111,* 8511−8513.

Lebioda, L., & Stec, B. (1991) *Biochemistry 30,* 2817−2822.

Lebioda, L., Stec, B., Brewer, J. M., & Tykarska, E. (1991) *Biochemistry 30,* 2823−2827.

Lebioda, L., Zhang, E., Lewinski, K., & Brewer, J. M. (1993) *Proteins: Struct., Funct., Genet. 16,* 219−225.

Lee, M. E., & Nowak, T. (1992) *Arch. Biochem. Biophys. 293,* 264−273.

Luzzati, V. (1952) *Acta Crystallogr. 5,* 802−810.

Malmström, B. G. (1961) *Enzymes, 2nd Ed. 5,* 471−494.

Perona, J. J., Craik, C. S., & Fletterick, R. J. (1993) *Science 261,* 620−621.

Petsko, G. A., Kenyon, G. L., Gerlt, J. A., Ringe, D., & Kozarich, J. W. (1993) *Trends Biochem. Sci. 18,* 372−376.

Poyner, R. R., & Reed, G. H. (1992) *Biochemistry 31,* 7166−7173.

Poyner, R. R., Laughlin, L. T., Sowa, G. A., & Reed, G. H. (1996) *Biochemistry 35,* 1692−1699.

Rodgers, D. W. (1994) *Structure 2,* 1135−1140.

Sangadala, V. S., Glover, C. V. C., Robson, R. L., Holland, M. J., Lebioda, L., & Brewer, J. M. (1995) *Biochim. Biophys. Acta 1251,* 23−31.
Sillén, L. G., & Martell, A. E. (1964) *Stability Constants of Metal-Ion Complexes*, Spec. Publ. No. 17, The Chemical Society, London.
Singer, P. T., Smalås, A., Carty, R. P., Mange, W. F., & Sweet, R. M. (1993a) *Science 259,* 669−673.
Singer, P. T., Smalås, A., Carty, R. P., Mange, W. F., & Sweet, R. M. (1993b) *Science 261,* 621−622.
Smith, T. J. (1990) *J. Appl. Crystallogr. 23,* 141−142.
Stec, B., & Ledioda, L. (1990) *J. Mol. Biol. 211,* 235−248.
Stubbe, J. A., & Abeles, R. H. (1980) *Biochemistry 19,* 5505−5512.
Teng, T.-Y. (1994) *J. Appl. Crystallogr. 23,* 387−391.
Terrill, J. B., & Reilley, C. N. (1966) *Anal. Chem. 38,* 1876−1881.
Tronrud, D. E., Ten Eyck, L. F., & Matthews, B. W. (1987) *Acta Crystallogr., Sect. A 43,* 489−501.
Wedekind, J. E., Poyner, R. R., Reed, G. H., & Rayment, I. (1994) *Biochemistry 33,* 9333−9342.
Wedekind, J. E., Reed, G. H., & Rayment, I. (1995) *Biochemistry 34,* 4325−4330.
Williams, D. H., & Busch, D. H. (1965) *J. Am. Chem. Soc. 87,* 4644−4645.
Wold, F., & Ballou, C. E. (1957) *J. Biol. Chem. 227,* 313−328.
Zhang, E., Lebioda, L., Chen, Y., Brewer, J. M., Hatada, M., & Minor, W. (1994a) *Acta Crystallogr. D50,* 335−336.
Zhang, E., Hatada, M., Brewer, J. M., & Lebioda, L. (1994b) *Biochemistry 33,* 6295−6300.

BI952859C